Eur. Phys. J. A **19**, 333–339 (2004)
DOI 10.1140/epja/i2003-10133-0

THE EUROPEAN PHYSICAL JOURNAL A

Evolution of Airy structure in ^{12}C(^{12}C, ^{12}C)^{12}C between 5 and 10 MeV/A

F. Michel[1,a] and S. Ohkubo[2]

[1] Faculté des Sciences, Université de Mons-Hainaut, B-7000 Mons, Belgium
[2] Department of Applied Science and Environment, Kochi Women's University, Kochi 780-8515, Japan

Received: 2 September 2003 / Revised version: 25 September 2003 /
Published online: 5 February 2004 –
Communicated by V. Vento

Abstract. We investigate the properties of a global optical potential, which describes the ^{12}C + ^{12}C elastic-scattering data between 70 and 130 MeV, within the nearside/farside and barrier-wave/internal-wave decomposition techniques. Particular emphasis is laid on the discussion of the incomplete absorption features of this system, and especially on the properties of the Airy minima which are observed in the experimental 90° excitation function. The complicated angular and energy evolution of the data is explained in terms of the interference of a small set of scattering subamplitudes with a much simpler behavior.

PACS. 24.10.-i Nuclear reaction models and methods – 24.10.Ht Optical and diffraction models – 25.70.Bc Elastic and quasielastic scattering

1 Introduction

The observation of Airy maxima and minima in the elastic-scattering angular distributions for some light heavy-ion systems, like ^{16}O + ^{16}O, ^{16}O + ^{12}C and ^{12}C + ^{12}C, has attracted much attention recently [1–5]. The appearance of these refractive features is considered to provide the most direct evidence for a substantial transparency of the interaction; this incomplete absorption makes possible a precise determination of the optical-model potential on a much broader radial range than is possible for systems dominated by strong absorption, for which the potential can only be investigated in the far surface region [6].

It has thus been found that the real part of potentials reproducing the evolution with energy of the Airy features of the data must necessarily be deep, in agreement with the predictions of semimicroscopic approaches like the folding model [7–10], or more microscopic calculations where antisymmetrization between projectile and target is fully taken into account [11]. Optical-model potentials, varying smoothly with energy and reproducing reasonably well the complicated energy dependence of the data, are now available for several of these exceptional systems [1–5]. A recent review, enhancing the incomplete-absorption features displayed by some light heavy-ion systems and the current optical-model understanding of these features, can be found in ref. [12].

[a] e-mail: francis.michel@umh.ac.be

The physics of the Airy extrema has often been discussed within the frame of semiclassical approaches. These techniques have revealed to be particularly helpful for disentangling the various interfering mechanisms involved in the building up of the scattering amplitude, which make the angular and energy dependence of the scattering cross-section very intricate; the situation is even more complex in the case of identical colliding nuclei, where the symmetrization of the scattering amplitude introduces additional interference effects. As an example, we display in fig. 1(a) the predictions, in 2 MeV steps between 70 and 130 MeV, of a global ^{12}C + ^{12}C phenomenological optical potential of Brandan *et al.* [5], which describes successfully the fourteen experimental angular distributions of Stokstad *et al.* [13] between 70.7 and 126.7 MeV. Whereas at small (and large) angles, the energy dependence of the angular-distribution pattern is smooth and well described in terms of diffraction effects, at intermediate angles the angular pattern is seen to vary wildly on a scale of a few MeV; at 90° the Brandan potential predicts a collapse of the cross-section around 80, 100 and 130 MeV; this is in qualitative agreement with the experimental 90° excitation function, which displays broad Airy minima around the first two of these energies [14], and the collapse of the experimental cross-section around 90° at 126.7 MeV [13]. Note that in fig. 1(a), as in other figures where the symmetrized cross-section is displayed, we present the ratio of the cross-section to the symmetrized Rutherford cross-section $\sigma_{\rm R}(\Theta) + \sigma_{\rm R}(\pi - \Theta)$, and not to

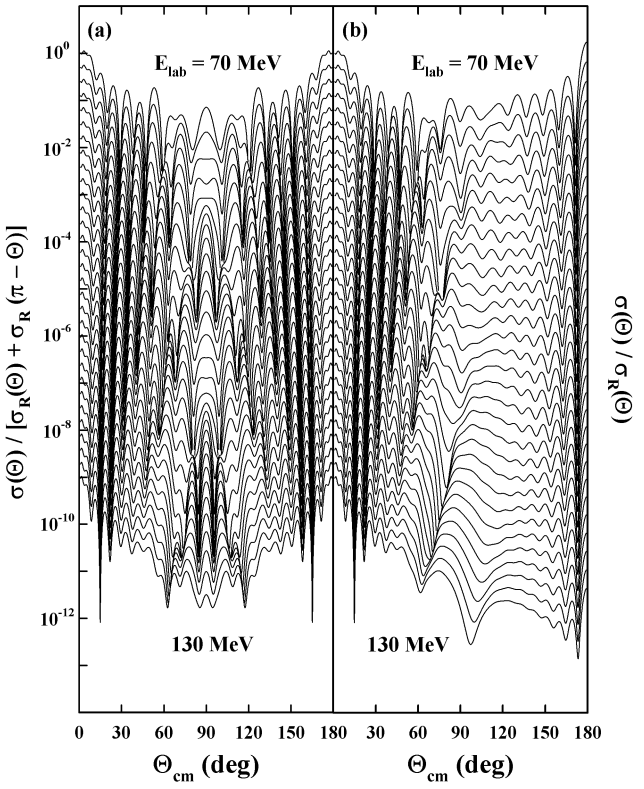

Fig. 1. Symmetrized (a) and non-symmetrized (b) ^{12}C + ^{12}C optical-model angular distributions calculated in 2 MeV steps between 70 and 130 MeV laboratory energies using the energy-dependent potential of Brandan *et al.* [5] (in this and the following similar figures, the 70 MeV curve is normalized correctly, and each successive curve is displaced by a factor of 2 with respect to the previous one).

the Mott cross-section, in order to avoid the introduction of additional unphysical oscillations in the plot due to the considerable structure present in the Mott cross-section at these energies [15].

In two recent papers [15,16], we have presented a thorough analysis of the ^{16}O + ^{16}O optical-model elastic angular distributions, for energies ranging from 5 to 10 MeV per nucleon, within the frame of the barrier-wave/internal-wave (B/I) separation technique; we showed that this decomposition, first introduced in a semiclassical context by Brink and Takigawa [17,18], complements nicely the picture supplied by the more popular nearside/farside (N/F) approach [19], and that it provides a much clearer and deeper explanation of the building-up of the Airy extrema seen in the 90° excitation function and in the angular distributions. By investigating this decomposition further, we have more recently shown [20] that the mechanism underlying the gross structure observed in light heavy-ion scattering is in fact rather different from that which produces the Airy structure in the meteorological rainbow, and that the Airy terminology is thus not fully adequate in the nuclear context; for convenience we will however stick to this widely used conventional terminology in the following.

In the N/F approach, the elastic-scattering amplitude, $f(\Theta)$, is split into two contributions, $f_{\rm N}(\Theta)$ and $f_{\rm F}(\Theta)$, corresponding to classical trajectories with positive and negative deflection angles, respectively [19]. While the Fraunhofer oscillations seen at small angles are found to result from the interference between the nearside and farside contributions to the scattering, the Airy structure seen in the experimental data for systems governed by incomplete absorption is found to be fully carried by the farside component.

To explain the Airy structure in this approach, one has thus to invoke the existence, in the farside component itself, of two interfering contributions corresponding to negative deflection angle trajectories with different ranges of angular momenta, usually noted as $\ell_<$ and $\ell_>$ [21]. This mechanism is similar to that proposed long ago by Airy to explain the supernumerary bows seen in the familiar meteorological rainbow. One observes that an increase of the imaginary part of the optical potential in the central region makes the Airy oscillations disappear [22]; this is interpreted as being due to the progressive damping of the lower angular-momentum contribution $\ell_<$ to $f_{\rm F}$ when absorption increases.

In the alternative B/I scheme —which makes only sense if the real part of the potential is deep enough for the effective potential to display a "potential pocket" for all the active partial waves— the elastic-scattering amplitude is also split into two parts: the barrier contribution, $f_{\rm B}(\Theta)$, which corresponds to the part of the flux which is reflected at the effective potential barrier, and the internal contribution, $f_{\rm I}(\Theta)$, which accounts for the part of the incident flux which penetrates the nuclear interior and re-emerges in the entrance channel after reflection from the most internal turning point [17,18].

Numerical experiments show that the internal contribution can give a sizeable contribution to the scattering amplitude when absorption is incomplete, while it becomes vanishingly small when absorption is strong. For systems like ^{16}O + ^{16}O, the internal component is indeed found to give an important contribution to the full scattering amplitude [15]. More importantly, the (non-symmetrized) barrier and internal contributions are found to have comparable magnitude and to behave smoothly in the angular region where the Airy extrema are observed. In the B/I picture, the appearance of the Airy structure is thus directly connected with an interference mechanism between the barrier and internal components of the scattering amplitude [15]; the B/I decomposition thus provides a much more direct interpretation of the Airy extrema than the N/F scheme.

It proves useful to combine these two approaches, and to extract the nearside and farside components of the barrier and internal contributions $f_{\rm B}$ and $f_{\rm I}$; this was first proposed in a pioneering paper by Rowley, Doubre and Marty for the ^{12}C + ^{12}C system at the c.m. energy of 51 MeV [23], and systematically applied to the ^{16}O + ^{16}O case in refs. [15,16]. In contrast with alternative approaches, like the so-called "interpolated-envelope technique" [24], where this decomposition is performed in

an empirical way, the N/F decomposition of the barrier and internal-wave amplitudes is performed in a rigorous way, and in addition it provides components with a clear physical content. This two-step decomposition eventually supplies the two smooth components of the farside contribution, $f_{\mathrm{B,F}}$ and $f_{\mathrm{I,F}}$, whose interference explains the structure seen in the farside contribution in the ^{16}O + ^{16}O case, and hence the Airy structure seen in the full elastic-scattering amplitude.

In ref. [15], this decomposition scheme was applied to the study of the properties of the ^{16}O + ^{16}O optical-model potential of Nicoli [25] between 75 and 124 MeV incident energy. The parameters of this potential were individually adjusted to experiment at each energy [25]; the potentials extracted all belong to a single potential family, which is smoothly connected to that fitting the elastic-scattering data up to the highest incident energies [4], and is thus determined in a unique way. Because of the relative stability of the parameters of the optical potential of ref. [25], it proved possible [15] to extract the general trends of the energy behavior of the various components of the ^{16}O + ^{16}O elastic-scattering amplitude; emphasis was laid on the angular and energy dependence of the non-symmetrized contributions to the cross-section.

In the present paper, we propose a systematic analysis for the ^{12}C + ^{12}C system between 70 and 130 MeV incident energy, where the differential cross-section pattern is also dominated by symmetrization effects; as a global optical potential is available for that system, it proves possible to obtain a much clearer and consistent picture of the energy evolution of the various contributions of the cross-section; this study will, we hope, give additional impetus to the systematic use of the barrier-wave/internal-wave decomposition technique in the analysis of light heavy-ion scattering data.

2 Analysis of ^{12}C + ^{12}C elastic scattering for incident energies between 70 and 130 MeV

2.1 The N/F and B/I decomposition techniques

We briefly recall here the essential ingredients and physical contents of the nearside/farside and barrier-wave/internal-wave decomposition techniques. Technical details and relevant references can be found, *e.g.*, in ref. [15]; for a general discussion on the use of semiclassical approaches in nuclear scattering problems, the reader is referred to the classical textbooks [18,26,27].

In the nearside/farside decomposition of Fuller [19], the elastic-scattering amplitude $f(\Theta)$ is decomposed into two subamplitudes $f_{\mathrm{N}}(\Theta)$ and $f_{\mathrm{F}}(\Theta)$ (nearside and farside components). The decomposition is performed by replacing the Legendre polynomials appearing in the partial-wave series for the amplitude by their "travelling wave" components $\tilde{Q}_\ell^{(+)}$ and $\tilde{Q}_\ell^{(-)}$, which are defined in terms of the Legendre polynomials P_ℓ and the Legendre functions of the second kind Q_ℓ:

$$\tilde{Q}_\ell^{(\pm)} = \frac{1}{2}\left[P_\ell(\cos\Theta) \mp i\frac{2}{\pi}Q_\ell(\cos\Theta)\right]; \qquad (1)$$

a similar decomposition, which can be performed analytically, has to be carried out for the Rutherford scattering amplitude.

One of the merits of the N/F decomposition technique is that it can be performed in an unambiguous way, starting from the exact (quantum) scattering amplitude. It has, however, been argued recently that it leads sometimes to the appearance of unphysical contributions in the near-side and farside contributions, which cancel out in the full amplitude, and improved N/F decompositions have been proposed [28]. As mentioned in the introduction, the most important drawback of the N/F approach in the present context is that it does not provide by itself an explanation of the Airy pattern, since the interference phenomenon we are interested in is embedded into one of the two components (the farside component) of the scattering amplitude.

The B/I decomposition technique turns out to bring more pertinent information in this case, since the interference between the barrier-wave and internal-wave subamplitudes fully explains the experimental interference pattern. In addition, an N/F decomposition of these two subamplitudes, which can be performed in a rigorous way using the transformation of eq. (1), provides eventually the barrier-wave and internal-wave components of the farside amplitude which are responsible for the interference seen in the latter. The B/I decomposition is technically rather straightforward to perform, since the semiclassical calculation initially proposed by Brink and Takigawa can be replaced by a succession of optical-model estimates [29].

2.2 The ^{12}C + ^{12}C global optical potential

In ref. [5], Brandan *et al.* carried out a folding-model analysis and a phenomenological analysis of the fourteen ^{12}C + ^{12}C complete angular distributions of Stokstad *et al.* [13] between 70.7 and 126.7 MeV incident energy. The latter analysis, on which we will concentrate in the following, made use of Woods-Saxon volume form factors for the real and imaginary parts of the potential $U(r)$:

$$U(r) = -\frac{V_0}{1+\exp((r-R_v)/a_v)} - i\frac{W_0}{1+\exp((r-R_w)/a_w)} + V_{\mathrm{c}}(r)\,, \qquad (2)$$

where $V_0 = 386.2 - 0.868E_{\mathrm{lab}}$, $R_v = 2.669$, $a_v = 0.902$, $W_0 = -8.19 + 0.208E_{\mathrm{lab}}$, $R_w = 8.393 - 0.0252E_{\mathrm{lab}}$, $a_w = -0.079 + 0.0057E_{\mathrm{lab}}$ (energies in MeV, lengths in fm); V_{c} is the Coulomb potential between two uniformly charged spheres with radius 3.17 fm (an alternative parametrization of the energy dependence of the potential, provided in ref. [5], will not be used here). Up to $E_{\mathrm{lab}}/A \simeq 10$ MeV, several real potential depths are compatible with the data,

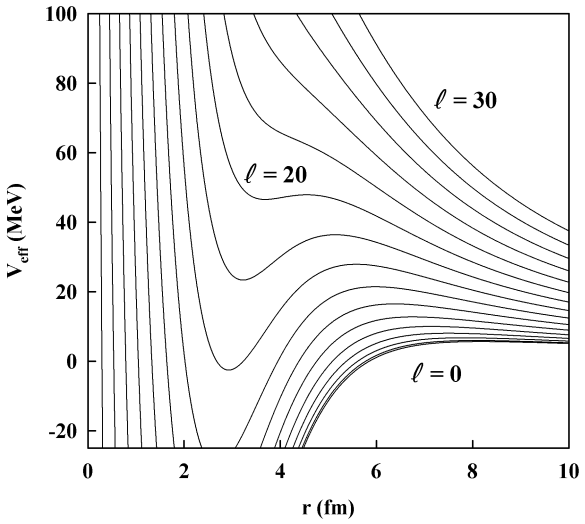

Fig. 2. Effective potential curves for angular momenta between 0 and 30, calculated at 100 MeV using the real part of the ^{12}C + ^{12}C optical potential of Brandan *et al.* [5].

but by imposing continuity with the results at higher energy, where the discrete ambiguity is resolved, a single potential family is obtained, with a real volume integral per nucleon pair, J_v, of about 350 MeV fm^3 around 100 MeV incident energy. The angular distributions presented in fig. 1 between 70 and 130 MeV in 2 MeV steps were obtained using the potential of eq. (2).

In fig. 1(b), we present the same angular distributions as in fig. 1(a), but without symmetrization of the optical-model scattering amplitude (and thus given as the ratio of the cross-section to the Rutherford cross-section). After elimination of the symmetrization interference effects, a more regular energy dependence is observed; the most striking feature is the apparition of several broad Airy minima, whose angular position shifts towards smaller angles as energy increases. The crossing of these minima at $\Theta = 90°$ produces the minima seen in the 90° experimental excitation function; although they are more difficult to see in the symmetrized angular distributions, a careful examination also reveals the existence of these minima at smaller (and larger) angles; for example, their influence on the symmetrized angular-distribution pattern is clearly seen around $E_{\rm lab} = 120$ MeV near 70° (and 110°).

2.3 The B/I decomposition of the ^{12}C + ^{12}C scattering amplitude

It is interesting to have a look at the real part of the effective potentials in the energy region of interest, that is between $E_{\rm c.m.} = 30$ and 60 MeV (fig. 2): the effective potential is seen to display pockets up to about $E_{\rm c.m.} = 50$ MeV. Up to that energy (and, as a matter of fact, slightly beyond), it is thus technically feasible to decompose the elastic-scattering amplitude into its barrier-wave and internal-wave components. This decomposition was carried out by using the perturbative technique of ref. [29],

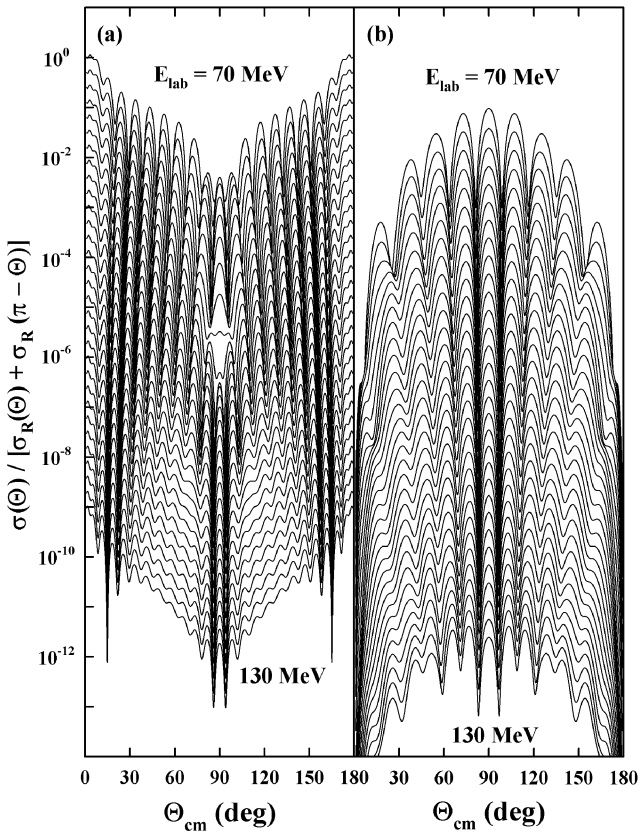

Fig. 3. Barrier-wave (a) and internal-wave (b) contributions to the symmetrized ^{12}C + ^{12}C cross-sections between 70 and 130 MeV laboratory energies.

that is, by examining the response of the elastic S-matrix to small modifications of the potential, localized in the region of the potential pocket. The accuracy of the calculations was checked by examining the stability of the results against modifications of the parameters of the perturbation.

The result of the decomposition is illustrated in fig. 3. In this figure we display the *symmetrized* barrier-wave and internal-wave cross-sections, which have rarely been presented in this context. The most remarkable result of our calculations is that the hectic behavior of the full symmetrized cross-section of fig. 1(a) is now replaced by two very orderly angular-distribution patterns; this proves that the B/I decomposition is indeed the most natural technique to investigate the scattering in this energy region. Around 90°, the internal-wave contribution dominates the scattering by more than one order of magnitude, while the diffractive regime at small and large angles is governed by the barrier-wave contribution. Interference effects can be seen around 90° in the barrier contribution, but they have little influence on the full cross-section because of the internal-wave dominance there; anecdotically, we note the presence of a minimum at 90°, which has to be interpreted as an interference effect between the nearside and farside components of the barrier-wave amplitude. More interesting to comment is the fact that the

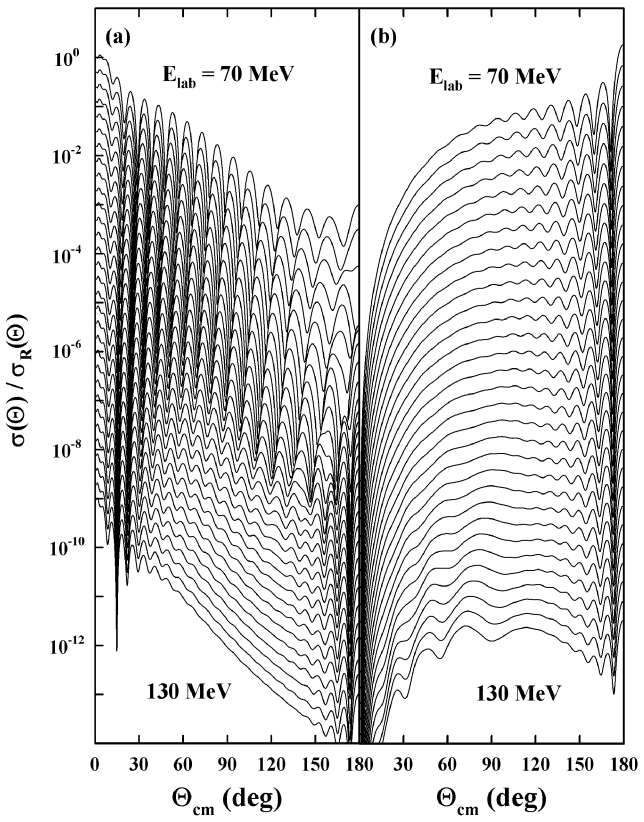

Fig. 4. Same as fig. 3 for the non-symmetrized ^{12}C + ^{12}C cross-sections.

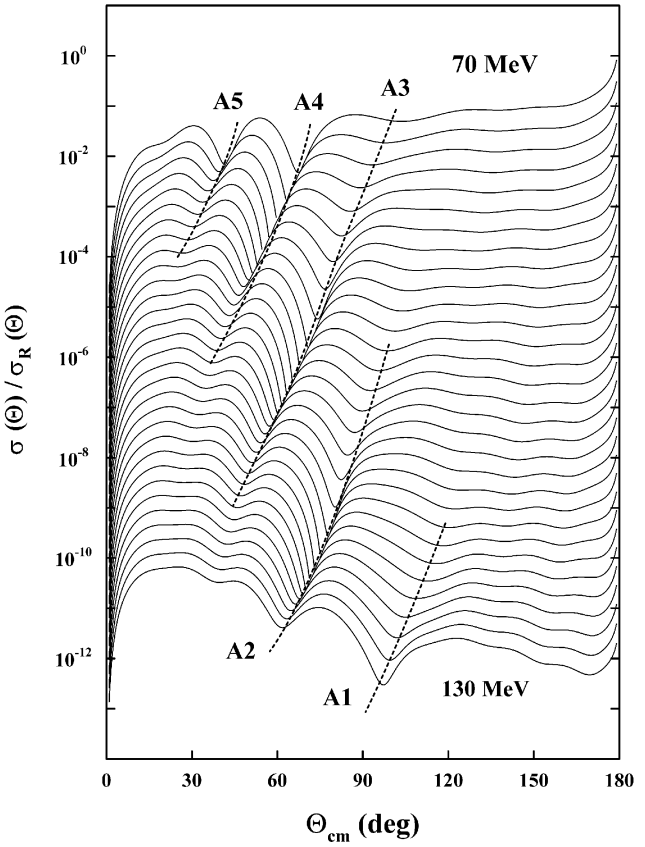

Fig. 5. Farside contributions to the non-symmetrized ^{12}C + ^{12}C cross-sections between 70 and 130 MeV laboratory energies. The dashed lines highlight the evolution with energy of the position of various Airy minima.

broad oscillations displayed by the internal-wave angular distribution are essentially symmetrization oscillations; indeed the non-symmetrized version of this angular distribution, which can be found in fig. 4(b), is essentially smooth in the intermediate angles region. As to the rise seen at large angles in the non-symmetrized internal-wave cross-section, which plays an all-important role in explaining the ALAS pattern seen at large angles in some light-ion scattering systems (see, *e.g.*, ref. [30]), it plays a very minor role here since, in the full angular distribution, it is essentially hidden by the Coulomb contribution in this angular region. A look at fig. 4(a) also shows in a vivid way the effect on the barrier-wave contribution of the progressive disappearance of the potential pocket around 50 MeV c.m. energy: the angular distribution becomes much smoother around 90°, and the oscillations seen in the symmetrized barrier-wave cross-sections in this angular region are thus essentially due to symmetrization interference effects at these energies.

2.4 Farside component of the ^{12}C + ^{12}C barrier-wave and internal-wave scattering amplitudes

Although from our point of view the B/I decomposition has richer physical contents in the present context, it is very useful to have a look at the results of the N/F decomposition technique, which is largely complementary to the former. For example, the energy evolution of the Airy minima of fig. 1(a) is much clearer in the farside contribution to the non-symmetrized scattering amplitude, as can be seen in fig. 5, because the latter does no more contain the component responsible for the appearance of the small-angles Fraunhofer oscillations. Between 70 and 130 MeV laboratory energy, five Airy minima can be discerned; they are labeled with their order in fig. 5 according to the usual convention (A1 is the last minimum to appear at large angles when energy increases); A1 to A3 are responsible for the three minima of the 90° excitation function discussed in the introduction. Note that A4 cannot play an important role in the energy range considered here, because it appears at too low an angle and is masked by the Fraunhofer oscillations; this remark is still more pertinent for A5.

It is seen that each of these Airy minima does not survive on the full energy range; for example, A3 is most noticeable between 80 and 100 MeV incident energy, while A1 appears only beyond about 120 MeV. This can be understood easily if one refers to the barrier-wave/internal-wave components of the farside component —or, more correctly, to the farside contribution to the barrier-wave and internal-wave components (fig. 6). Indeed, it is seen that whereas the slope of the farside/barrier component

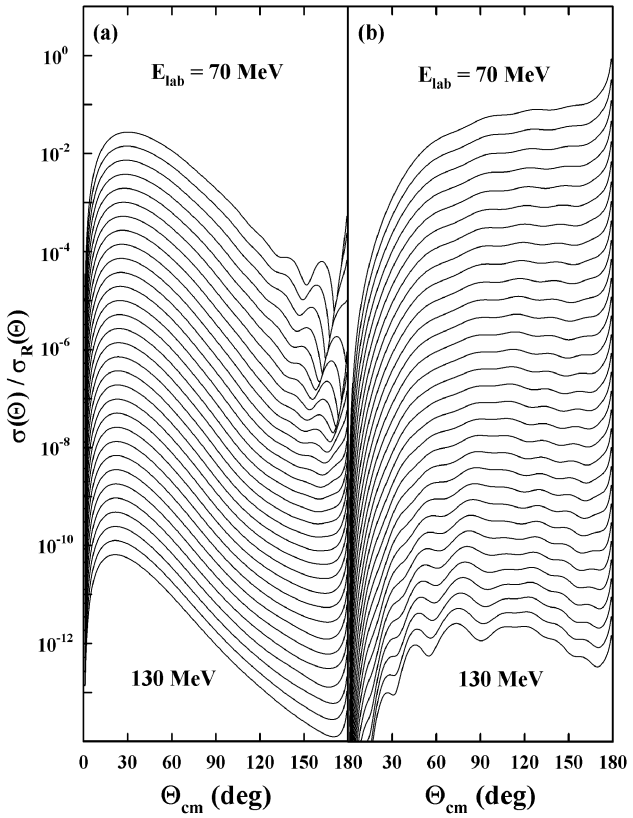

Fig. 6. Farside contribution to the barrier-wave (a) and internal-wave (b) components of the non-symmetrized $^{12}C + {}^{12}C$ cross-sections between 70 and 130 MeV.

is essentially independent of energy, this is not the case for the farside/internal contribution; the angle where both amplitudes are comparable, and where interference effects are thus expected be enhanced, is seen to increase with energy, in accordance with the results of fig. 5. Figure 6 also shows that the oscillatory behavior of the (non-symmetrized) barrier-wave contribution, and of the internal-wave contribution at large angles (fig. 4) is essentially due to interference effects with their nearside component.

3 Conclusions

In this paper, we have investigated the properties of the global optical potential of Brandan *et al.* [5], which describes consistently the $^{12}C + {}^{12}C$ elastic-scattering data of Stokstad *et al.* [13] between 70 and 130 MeV incident energies, by decomposing the optical-model scattering amplitude into its nearside/farside and barrier-wave/internal-wave components. The presence of a substantial internal-wave contribution, which interferes with the barrier-wave component to generate the observed Airy minima, emphasizes the incomplete-absorption features of this system. The most spectacular result of the analysis is to provide an explanation of the intricate angular and energy evolution of the data in terms of the interference of a small set of scattering subamplitudes with a much simpler behavior and an intuitively appealing interpretation.

We believe that the barrier-wave/internal-wave decomposition technique, which is very simple to implement in any standard optical-model code, should be applied in a more systematic way —together with more conventional approaches like the nearside/farside decomposition— in the analysis of light heavy-ion scattering.

S.O. thanks W. von Oertzen, H.G. Bohlen and Dao T. Khoa for useful discussions. S.O. has been supported by a Grant-in-aid for Scientific Research of the Japan Society for Promotion of Science (No. 12640288).

References

1. M.P. Nicoli, F. Haas, R.M. Freeman, S. Szilner, Z. Basrak, A. Morsad, G.R. Satchler, M.E. Brandan, Phys. Rev. C **61**, 034609 (2000).
2. A.A. Ogloblin, Yu.A. Glukhov, W.H. Trzaska, A.S. Dem'yanova, S.A. Goncharov, R. Julin, S.V. Klebnikov, M. Mutterer, M.V. Rozhkov, V.P. Rudakov, G.P. Tiorin, Dao T. Khoa, G.R. Satchler, Phys. Rev. C **62**, 044601 (2000).
3. M.P. Nicoli, F. Haas, R.M. Freeman, N. Aissaoui, C. Beck, A. Elanique, R. Nouicer, A. Morsad, S. Szilner, Z. Basrak, M.E. Brandan, G.R. Satchler, Phys. Rev. C **60**, 064608 (1999).
4. Dao T. Khoa, W. von Oertzen, H.G. Bohlen, F. Nuoffer, Nucl. Phys. A **672**, 387 (2000).
5. M.E. Brandan, M. Rodríguez-Villafuerte, A. Ayala, Phys. Rev. C **41**, 1520 (1990).
6. G.R. Satchler, *Direct Nuclear Reactions* (Clarendon Press, Oxford, 1983).
7. G.R. Satchler, W.G. Love, Phys. Rep. **55**, 183 (1979) and references therein.
8. Dao T. Khoa, W. von Oertzen, H.G. Bohlen, Phys. Rev. C **49**, 1652 (1994).
9. Dao T. Khoa, G.R. Satchler, W. von Oertzen, Phys. Rev. C **56**, 954 (1997).
10. Dao T. Khoa, G.R. Satchler, Nucl. Phys. A **668**, 3 (2000).
11. H. Horiuchi, in *Trends in Nuclear Physics*, edited by P.J. Ellis, Y.C. Tang (Addison-Wesley, Reading, Mass., 1991) p. 277.
12. M.E. Brandan, G.R. Satchler, Phys. Rep. **285**, 143 (1997) and references therein.
13. R.G. Stokstad, R.M. Wieland, G.R. Satchler, C.B. Fulmer, D.C. Hensley, S. Raman, L.D. Rickertsen, A.H. Snell, P.H. Stelson, Phys. Rev. C **20**, 655 (1979).
14. A. Morsad, F. Haas, C. Beck, R.M. Freeman, Z. Phys. A **338**, 61 (1991).
15. F. Michel, G. Reidemeister, S. Ohkubo, Phys. Rev. C **63**, 034620 (2001).
16. F. Michel, F. Brau, G. Reidemeister, S. Ohkubo, Phys. Rev. Lett. **85**, 1823 (2000).
17. D.M. Brink, N. Takigawa, Nucl. Phys. A **279**, 159 (1977).
18. D.M. Brink, *Semi-classical Methods for Nucleus-Nucleus Scattering* (Cambridge University Press, Cambridge, 1985).
19. R.C. Fuller, Phys. Rev. C **12**, 1561 (1975).

20. F. Michel, G. Reidemeister, S. Ohkubo, Phys. Rev. Lett. **89**, 152701 (2002).
21. K.W. McVoy, G.R. Satchler, Nucl. Phys. A **417**, 157 (1984).
22. K.W. McVoy, H.M. Khalil, M.M. Shalaby, G.R. Satchler, Nucl. Phys. A **455**, 118 (1986).
23. N. Rowley, H. Doubre, C. Marty, Phys. Lett. B **69**, 147 (1977).
24. R. Da Silveira, Ch. Leclercq-Willain, Z. Phys. A **314**, 63 (1983).
25. M.P. Nicoli, Thesis, Strasbourg, 1998 (Int. Rep. IReS 98-16).
26. W.E. Frahn, *Diffractive Processes in Nuclear Physics* (Clarendon Press, Oxford, 1985).
27. H.M. Nussenzveig, *Diffraction Effects in Semiclassical Scattering* (Cambridge University Press, Cambridge, 1992).
28. R. Anni, J.N.L. Connor, C. Noli, Phys. Rev. C **66**, 044610 (2002).
29. J. Albinski, F. Michel, Phys. Rev. C **25**, 213 (1982).
30. F. Michel, S. Ohkubo, G. Reidemeister, Prog. Theor. Phys. Suppl. **132**, 7 (1998).